HHS Public Access

Author manuscript

J Shoulder Elbow Surg. Author manuscript; available in PMC 2023 November 01.

Published in final edited form as:

J Shoulder Elbow Surg. 2022 November ; 31(11): 2366–2380. doi:10.1016/j.jse.2022.05.004.

Tendon Progenitor Cells as Biological Augmentation Improve Functional Gait and Reduce Scar Formation after Rotator Cuff Repair

Alexander J Vervaecke, MD[1,2,4], **Andrew D Carbone, MD**[1], **Adam Abraham, PhD**[3], **Zachary Bernstein**[1], **Damien Laudier**[1], **Olivier Verborgt, MD, PhD**[2,4], **Leesa M Galatz, MD**[1], **Alice H. Huang, PhD**[5]

[1]The Mount Sinai Hospital, Department of Orthopaedics, New York, NY, USA

[2]Faculty of Medicine and Health Sciences, University of Antwerp, Antwerp, Belgium

[3]University of Michigan, Department of Orthopaedics, Ann Arbor, MI, USA

[4]Orthopaedic Center Antwerp, AZ Monica, Antwerp, Belgium

[5]Columbia University, Department of Orthopedic Surgery, New York, NY, USA

Abstract

Background: High rates of structural failure are reported after rotator cuff repairs due to inability to recreate the native enthesis during healing. The development of biological augmentation methods that mitigate scar formation and regenerate the enthesis is still an unmet need. Since neonatal enthesis is capable of regeneration after injury, this study tested whether delivery of neonatal tendon progenitor cells (TPC) into the adult injured environment can enhance functional and structural supraspinatus enthesis and tendon healing.

Methods: TPCs were isolated from Ai14 Rosa26-TdTomato mouse Achilles tendons and labeled using Adenovirus-Cre. 52 CB57BL/6J mice underwent detachment and acute repair of the supraspinatus tendon and received either a fibrin-only or TPC-fibrin gel. Immunofluorescence analysis was carried out to determine cellularity (DAPI), fibrocartilage (SOX9), macrophages (F4/80), myofibroblasts (αSMA), and scar (laminin). Assays for function (gait and biomechanical testing) and structure (μCT imaging, Picrosirius Red/Alcian Blue staining, type I and III collagen staining) were carried out.

Corresponding Authors: Alice H. Huang, PhD ah364@cumc.columbia.edu, Columbia University, Department of Orthopedic Surgery, 650 W 168th Street, New York, NY 10032, USA, - OR - Leesa M. Galatz, MD leesa.galatz@mountsinai.org, Mount Sinai Hospital, Department of Orthopaedics, 1468 Madison Ave, New York, NY 10029, USA.

Disclaimers:

Conflicts of interest: Dr. Galatz serves as a consultant for Medacta. Dr. Verborgt serves as a consultant for Zimmer-Biomet. The other authors, their immediate families, and any research foundation with which they are affiliated have not received any financial payments or other benefits from any commercial entity related to the subject of this article.

Level of Evidence: Basic Science Study; In Vivo Animal Model

Results: Analysis of TdTomato cells after injury showed minimal retention of TPCs by d7 and d14, with detected cells localized near the bursa and deltoid rather than the enthesis/tendon. However, TPC delivery led to significantly increased %Sox9+ cells in the enthesis at d7 post-injury and decreased laminin intensity across almost all time points compared to fibrin-only. Similarly, TPC-treated mice showed gait recovery by d14 (paw area and stride length) and d28 (stance time) while fibrin-treated mice failed to recover gait parameters. Despite improved gait, biomechanical testing showed no differences between groups. Structural analysis by μCT suggests that TPC application improves cortical thickness after surgery compared to fibrin. Superior collagen alignment at the neo-enthesis was also observed in the TPC-augmented group at d28, but no difference detected in type I and III collagen intensity.

Conclusion: We found that neonatal TPCs improved and restored functional gait by reducing overall scar formation, improving enthesis collagen alignment and altering bony composition response after supraspinatus tendon repair. TPCs did not appear to integrate into the healing tissue, suggesting improved healing may be due to paracrine effects at early stages. Future work will determine the factors secreted by TPCs to develop translational targets.

Keywords

rotator cuff tear; rotator cuff repair; biological augmentation; tendon progenitor cells; shoulder surgery; enthesis; scar formation; functional healing

Arthroscopic rotator cuff repairs can result in satisfactory improvements in pain and function scores. However, data also suggest a stagnation of success rates, with structural failures consistently reported in 15–25% of patients,[9,25,26,49] with even higher failure rates observed in older patients or those with massive rotator cuff tears (up to 94%).[12,53] While those with retears may still exhibit significant improvements compared to preoperatively,[19,34] long-term follow-up studies note functional declines in cases where rotator cuff integrity did not remain intact.[51] Select symptomatic patients with shoulder dysfunction may even necessitate revision surgery to properly restore their activity and function, which further highlights the importance of achieving structural healing in the index rotator cuff repair.[4,23,48] Unmodifiable biological characteristics such as tear size, retraction and chronicity, fatty infiltration, muscle atrophy and patient age and sex are all vital determinants of success. To optimize operative treatment, patient selection is therefore critical.[1,8,9,31,] Extensive research has been performed to establish repair procedures with a suitable biomechanical profile that maximizes healing.[28,45] Despite these efforts, the inability to recreate the native functional tendon-bone attachment remains an ongoing fundamental limitation.

In the uninjured shoulder, the rotator cuff attaches to its osseous footprint through a specialized interface termed the enthesis.[18] Consisting of four distinct zones (tendon, unmineralized fibrocartilage, mineralized fibrocartilage and bone), the enthesis functions to dissipate the high mechanical stresses that generally occur between tissues with divergent material properties (tendon and bone). Rotator cuff repair techniques entail reattaching the tendon to its insertion point with bone anchors. However, the native structure of the tendon-bone interface is not restored and healing occurs via the formation of disorganized fibrovascular scar tissue.[10,54] Consequently, the ability to distribute load transfer is lost, which predisposes the tissue to recurrent tears.[22] Several biological augmentation

approaches have been previously investigated to address this concern, including the application of platelet-rich plasma and mesenchymal stem cells; however, these therapies remain controversial with mixed success.[7,16,35,37] Thus, developing novel treatments that mitigate scar formation and regenerate enthesis structure and function remains an unmet critical need.

Enthesis development is regulated by a complex interaction of key molecular factors and mechanical loading cues that guide progenitor cells through differentiation and maturation.[13,44] Interestingly, during the early postnatal stage of enthesis development, neonatal enthesis cells retain the ability to regenerate the enthesis in response to scratch injury.[39] Similarly, neonatal tendon cells are recruited following complete Achilles tendon transection and regenerate a functional neo-tendon.[17] In contrast, similar injuries in adult mice do not lead to functional healing of either enthesis or tendon, and adult enthesis and tendon cells remain quiescent or differentiate abnormally.[17,39] Inducible lineage tracing of adult enthesis fibrocartilage (*Sox9*-lineage) and tendon (*Scx*-lineage) cells showed minimal participation in the resulting scar tissue after supraspinatus injury/repair highlighting the limited regenerative potential of intrinsic adult cells.[33,32] Although these studies suggest that unique properties in intrinsic neonatal cells underlie regenerative capacity, it may also be due to the unique systemic environment of the neonate. Therefore, to test the innate regenerative ability of neonatal cells within the adult environment, we delivered labeled neonatal tendon progenitor cells (TPCs) into the adult injured enthesis using a previously established mouse model of supraspinatus tendon detachment and repair. [32] We hypothesized that delivered TPCs would directly participate in tissue repair and improve structural and functional outcomes.

METHODS

Study design

52 male C57BL/6J mice (12 weeks old, Jackson Laboratory, Bar Harbor, ME) underwent detachment and acute repair of the left supraspinatus tendon.[2,32] At the time of the repair, mice were randomly allocated and received either a fibrin-only (n=26) or TPC-fibrin (n=26) gel (Figure 1A). To enable the detection of delivered cells, TPCs were labeled prior to encapsulation using the Ai14 Rosa-TdTomato (RosaT) reporter as described below. Animals were randomized into one of three assay subgroups, including: (1) cellular analyses by immunofluorescence at d7, 14, 28 (n=4); (2) functional analyses by gait (d0 preop, 7, 14, 28, n=10, non-terminal), biomechanical, and μCT testing at d28 (n=10, terminal) and (3) structural analyses by tinctorial and collagen staining at d28 (n=4) (Figure 1). To establish baseline comparative values for biomechanical testing and μCT and structural analysis, n=10 and n=2 contralateral uninjured shoulders were used per analysis group, respectively. All procedures were carried out according to approved IACUC guidelines at Mount Sinai.

TPC Isolation

Neonatal TPCs (postnatal day 7) were isolated from Ai14 Rosa-TdTomato Cre reporter (RosaT) mice.[30] Achilles tendons were digested in DMEM containing 1 mg/mL collagenase I and 5 mg/mL collagenase IV. Released cells were plated in growth media (DMEM

containing 10% FBS and 5% penicillin/streptomycin). At 70% confluence, cells were cryopreserved and expanded up to two passages post-thaw prior to use.

Adenovirus-mediated cell labeling

Adenoviruses for red fluorescent protein (Ad-RFP) and Cre recombinase (Ad-Cre) (Vector Biolabs, Malvern, PA, USA) were applied at a multiplicity of infection (MOI) 0, 10, 100 and, 200. After three days, TPCs were fixed in 4% paraformaldehyde and stained with DAPI. RFP+ or RosaT+ cells and DAPI+ nuclei were quantified in 3 representative images per well, and the number of RFP+/DAPI+ and RosaT+/DAPI+ cells was determined.

TPC-fibrin gels for delivery

TPCs were treated with Ad-Cre at MOI 100 to label cells by RosaT expression. 700K TPCs were then suspended in 17.5 uL of a 1:1 fibrin (10 mg/mL, Sigma Aldrich, Saint Louis, MO, USA) and MEM-α (ThermoFisher Scientific, Waltham, MA, USA) solution. 1 uL thrombin (25 U/mL) was added and 2.5 uL droplets pipetted in a sterile dish to form rounded beads (~1mm diameter, 100K cells/bead). Beads were subsequently stored in a humidified 37°C incubator until implantation (up to ~1 hr after encapsulation). Acellular fibrin beads were formulated similarly and maintained under similar conditions before use.

Surgical procedure

Anesthesia was induced with 3% isoflurane (Baxter, Deerfield, IL USA) with high-flow oxygen inhalation (2L/min) and maintained at 1.5% throughout surgery. Prior to incision, preoperative pain management was provided with a subcutaneous injection of buprenorphine (0.05 mg/kg, Buprenex). The mice were installed in a contralateral decubitus position with the ipsilateral forelimb fixated in external rotation and 75° of shoulder elevation under an overhead surgical microscope (Zeiss, Oberkochen, Germany). The surgical site was prepped, and a 1 cm skin incision was created over the lateral aspect of the acromion (Figure 1B). To expose the supraspinatus tendon, the deltoid muscle was partially detached from its acromial insertion. Using a Prolene 8.0 suture (Ethicon, Somerville, NJ, USA), a horizontal modified figure 8 stitch was used to secure the tendon just distal to the musculotendinous junction. The tendon was then sharply released from its insertion site, using a No. 11 surgical blade. Full detachment was verified by assessing the free movement of the tendon and by obtaining a clear view into the joint. Using a 30-gauge needle (Exelint Int., Redondo Beach, California), a posterior to anterior trans-osseous tunnel was manually drilled through the proximal humerus narrowly lateral to the level of the original insertion and parallel to the native supraspinatus enthesis site. The suture was passed through the bone tunnel from anterior to posterior and tied securely to approximate the supraspinatus to its native insertion site. Thereafter, a single gel bead was placed at the greater tuberosity. Finally, the deltoid muscle was reattached (8.0 Prolene), and the skin closed (6.0 Prolene). Mice returned to normal cage activity without immobilization. Postoperative analgesia was given 24h post-surgery (Buprenex, 0.05 mg/kg).

Cell analyses by immunofluorescence

Shoulders were dissected and the subscapular, infraspinatus and teres minor tendons were carefully detached. The samples were fixed in 4% paraformaldehyde, decalcified in EDTA, processed with 5% and 30% sucrose, embedded in optimum cutting temperature medium and subsequently frozen at −80°C. Alternating coronal cryosections (12 μm) were collected at the level of the supraspinatus enthesis site. Toluidine Blue staining was performed on adjacent sections to verify the correct anatomical region of each sample. Subsequently, immunostaining for cellularity (DAPI), fibrocartilage cells (Sox9), macrophages (F4/80; d7 only) and scar tissue/myofibroblasts (Laminin and α-smooth muscle actin; α-SMA) was carried out and samples were imaged (Zeiss AxioImager with optical sectioning by Apotome). Microscope exposure was kept consistent across all samples. For quantification, two representative regions of interest (ROIs) representing the newly repaired tendon-bone attachment (neo-enthesis) and the distal tendon-scar tissue were selected based upon morphological evaluation of Toluidine Blue and DAPI staining (Figure 2). The ROIs were quantified with ImageJ; DAPI, Sox9, and RosaT+ cells were quantified by manual counting using the CellCounter tool. For F4/80, laminin, and α-SMA stains, corrected total fluorescence intensities (CTFI) were calculated as the Integrated density – (area of interest (mm^2) x mean background fluorescence intensity) in raw greyscale images after applying correct scaling (466 px = 0.2 mm). Two coronal cryosections per shoulder were analyzed (100–200 μm apart) and means were calculated.

Gait analysis by high-speed motion capturing.

Gait analysis was carried out using the DigitGait Imaging System (Mouse Species Inc., Quincy, MA, USA) at d0 (preop), d3, d7, d14 and, d28. A high-speed digital camera (150 fps) captured the ventral position of each paw on a transparent treadmill (neutral inclination) while mice were gaited at a speed of 10 cm/s for 4 sec. Two independent registrations per mouse were performed per timepoint. Thereafter, the footage was analyzed using the DigiGait Analysis Software (DigiGait 12.4) and a semi-automatic correction of registration artifacts was executed. The parameters obtained for each forelimb were: Paw area at peak stance (cm^2), Stride length (cm) and Stance time (s). Mean values of the independent registrations were calculated.

Bone analysis by μCT scan

Humeri were dissected until only the supraspinatus tendon, muscle and repair construct remained attached to the humeral bone. Subsequently, they were wrapped in gauze, placed in custom 3D printed holders which were inserted to a 50mL conical tube (Falcon), filled with phosphate buffered saline and then placed in the μCT scanner (SkyScan 1176, Bruker). The following settings were used: X-ray tube potential 50 kV, X-ray intensity 500 μA, 0. 5 mm aluminum filter, frame averaging 2, rotation step 0.3°, resolution 8.93 μm. Scans were reconstructed using Bruker software (nRecon) and analyzed using Dragonfly image analysis software with the bone analysis plug in (Object Research Systems). The epiphysis was manually segmented by applying an Otsu threshold then sealing the ROI to the bone surface. The cortical and trabecular layers were then automatically segmented using the method described by Buie et al.[5] Bone morphometry outcome measurements included: Bone

volume fraction (calculated as bone-volume divided by total-volume), cortical thickness, cortical area fraction (calculated as cortical area divided by total area), trabecular separation, trabecular thickness and trabecular bone mineral density (BMD).

Biomechanical analysis by load frame testing

After μCT, the cross-sectional area of the tendons was determined using photogrammetry. In brief, humeri were placed in 3D printed grips that allowed the tendons to hang freely, samples were rotated using a stepper motor and a digital camera (CS165CU, Thorlabs) was used to take 40 pictures per revolution. Surface meshes of the tendon volume were obtained from the recorded images using commercial software (Agisoft Metashape) and then analyzed using Dragonfly to determine the cross-sectional area along the length of the tendon. The minimum cross-sectional area was then recorded and used to calculate material properties. Specimens were then further dissected by removing the supraspinatus muscle and placed in custom 3D-printed molds that encapsulate the humeral diaphysis.[24] The molds were gripped using custom tooling and the tendon was pulled until failure at a rate of 0.1% strain/second using a Mach-1 mechanical tester (Biomomentum). The force was applied parallel to the long axis of the humeral shaft. Samples were kept hydrated with phosphate buffered saline using a heated water bath set to 37°C. Displacement and force were recorded at 100 Hz. The structural properties determined were maximum force, yield force, stiffness, and work. The stiffness was determined from the maximally linear region of the force/displacement data using random sample consensus (RANSAC) implemented in a custom Matlab (Mathworks) script. Work was determined by computing the area under the force/displacement curve. Engineering stress and strain were computed using the cross-sectional area measured by photogrammetry and the initial specimen gauge length measured from the enthesis to the tendon grip tooling. The material properties determined were ultimate stress, yield stress, Young's Modulus, and Modulus of Resilience.

Structural analyses by tinctorial staining and immunohistochemistry

To best preserve structural morphology, dissected shoulders were processed at d28 for plastic embedding and sectioning. Shoulders were fixed in zinc formalin, dehydrated and infiltrated with methacrylate monomer and embedded. Coronal sections (6 μm) were acquired at representative levels of the supraspinatus enthesis, stained with Toluidine Blue and Alcian Blue/Picrosirius Red and imaged using light microscopy (Leica DM6B). Collagen fibril organization was assessed with polarized light and quantified in the two ROIs with the CTFI, with higher intensities suggesting improved organization.[14,20,42] The Image J FibrilTool plug-in was used to determine collagen fibril anisotropy.[3] Finally, to determine the contribution of collagen types I and III to the healing tissue, immunohistochemical staining was carried out with DAB and AEC chromogen detection. Images were quantified by calculating the optical density scores (ODS) with IHC Profiler.[43] Collagen I was assessed after running the built-in DAB color deconvolution module and collagen III staining was determined by performing chromogen color conversion and assessed with subsequent color deconvolution for eosine.

Statistical analyses

Pre-study power analysis with power β=0.8 and α=0.05 was performed to determine intervention and assay group sizes. Our primary hypothesis was that TPC treatment would improve chondrogenesis, reduce scar, enhance function (gait and mechanical properties) compared to fibrin treatment. The parameters used to estimate minimum sample size for each assay are included in Table 1. Estimated differences of means and coefficients of variation were based on our prior experimental datasets using this injury model.[32] Intragroup and intergroup differences for gait analysis were assessed using paired t-tests and 2-way ANOVA with Tukey's posthoc testing, respectively. Comparisons between groups for micro-CT, biomechanical and cell quantification parameters were assessed using mixed-effect (2-way ANOVA) models with Tukey or Fisher's LSD testing. All statistical analyses were performed using GraphPad Prism. Data are reported as mean±standard deviation.

RESULTS

Adenovirus Cre recombinase labels RosaT TPCs at MOI 100 and 200

Cells treated with Ad-RFP and Ad-Cre at MOI 0 showed no cell labeling. Increasing the MOI dose increased cell labeling only for Ad-Cre (Supplemental figure 1). MOI 100 (29.5 ± 5.9%) and 200 (47.1 ± 21.2%) had significantly higher percentages of RosaT+/DAPI+ cells compared to a MOI 10 (p=0.0015 and p=0.0038, respectively). No significant differences were found between the MOI 100 and 200 (p=0.16) for Ad-Cre. Due to the smaller variation in cell labeling and decreased risk of affecting cell viability compared to MOI 200, we opted to label TPCs with Ad-Cre at MOI 100.

TPC delivery increases early Sox9+ cells at the neo-enthesis and reduces overall scar markers

Immunofluorescence images were quantified at two ROIs representing the new enthesis (neo-enthesis) and tendon/scar regions (Figure 2). TPC delivery led to a transient increase in cellularity at the tendon-scar region at d14 (p=0.019), with no difference in cellularity at the neo-enthesis at any timepoint. While no differences were detected in Sox9+ fibrocartilage cells at the tendon-scar region at any timepoint, we observed an increase in %Sox9+ cells at d7 at the neo-enthesis region (p=0.021) (Figure 3). Analysis of scar markers laminin (extracellular matrix) and α-SMA (myofibroblast cells) showed diminished scar matrix formation with TPC treatment but minimal differences in scar-forming cells. Laminin immunostaining intensities were significantly decreased across all timepoints at the tendon-scar region (p=0.0059, p=0.033 and p=0.037 for d7, d14 and d28, respectively) and at d14 and d28 at the repaired enthesis site (p=0.0042 and p=0.0064, respectively). In contrast, while α-SMA intensities diminished over time for both ROIs, a significant difference was only observed between fibrin and TPC treatments for the neo-enthesis at d7 (p=0.0038) (Figure 4).

Analysis of RosaT+ cells showed minimal retention of labeled cells at d7; detected cells mainly were localized at the deltoid muscle or proximal tendon regions (Supplemental figure 2). Since TPCs did not engraft, but reduced scar matrix deposition was observed, we considered the possibility that TPCs may exert an immune effect on the adult injury

environment. Quantification of macrophages at d7 using the marker F4/80+ however, did not show any difference with TPC treatment (Supplemental figure 3).

Delivered TPCs restore functional gait after supraspinatus repair

To determine functional recovery, gait analysis was performed pre-(d0) and postop (d3–28) (Figure 5). Intragroup comparisons showed that mice receiving fibrin-only treatment did not fully recover gait function. While paw area in the fibrin-only group recovered by d14, stride length and stance time parameters remained impaired at all postop timepoints relative to preop. In contrast, TPC delivery resulted in recovery by d14 (paw area and stride length) and d28 (stance time). Comparing TPC and fibrin-only treatments directly, no differences were found in preop d0 values between treatment groups, indicating consistent starting baselines. Further intergroup comparisons showed that TPC delivery generally improved gait parameters relative to fibrin-only treatment, with persistent differences detected for stride length and stance time at d14 and d28.

Cortical and trabecular bone thickness remains unaltered to presurgical levels after TPC application

To determine bony changes to the humeral head after surgery, μCT was performed at d28 (Figure 6). While no differences were found for bone volume fraction, cortical area fraction, trabecular spacing, or bone mineral density between the two surgical groups, cortical bone thickness and trabecular thickness was lower in the TPC group compared to the fibrin-only ($p=0.0098$ and $p=0.0039$, respectively). Cortical thickness was comparable between TPC and nonsurgical control ($p=0.81$) but not for fibrin vs control ($p=0.042$). In contrast, trabecular thickness was significantly different for both fibrin and TPC groups compared to nonsurgical controls ($p<0.0001$ and $p=0.018$, respectively). Overall, this suggests that TPC application generally leads to improved bony response after rotator cuff repair in comparison to fibrin, but does not fully restore bony composition compared to nonsurgical controls.

Biomechanical tendon properties are not restored after augmentation

Biomechanical testing of the supraspinatus tendon-bone attachment at d28 showed no differences between fibrin-only and TPC-treatment. Further, all structural and material properties remained significantly reduced compared to intact non-surgical controls, with the exception of cross-sectional area (Figure 7).

TPCs improve collagen orientation at the enthesis site

To determine structural recovery, we assessed enthesis structure and collagen organization by tinctorial staining of plastic sections. Toluidine Blue staining revealed variable fibrocartilage formation at the repaired enthesis site in both groups. However, after injury, characteristic enthesis organization was not regenerated (Figure 8). Collagen organization was determined using Picrosirius Red staining and polarized light imaging. We found that TPC-augmented repairs had superior collagen alignment at the enthesis compared to the fibrin group ($p=0.045$), however no differences in anisotropy index were detected between groups. To semi-quantitively assess the fractions of collagen I and collagen III present at the ROIs, optical density scores were compared between groups. Overall, no differences were

found between the groups in the tendon and enthesis ROI for either collagen I (p=0.075; p=0.144, respectively) or collagen III (p=0.201; p=0.862, respectively) (Figure 9).

DISCUSSION

In this study, we determined whether neonatal TPCs maintain this unique regenerative capacity within the adult rotator cuff injury environment. Our primary findings were that TPC-treated adult mice fully restored functional gait, which may be due to reduced laminin scar formation, enhanced enthesis fibrocartilage cell number, altered humeral cortical and trabecular bone response and improved enthesis collagen orientation. Despite improved healing, TPC delivery did not completely restore the characteristic enthesis organization and tendon tensile properties remained significantly impaired. These latter findings are consistent with other attempted biological augmentation strategies applied for rotator cuff repair; to date, full regeneration of enthesis structure with full functional restoration remains an unmet goal.[6,38]

After reattachment of the rotator cuff tendon to the greater tuberosity, healing occurs through robust formation of fibrovascular scar tissue with an abrupt boundary between the healing soft tissue and bone.[29] Previous reports demonstrated that α-SMA-lineage cells are rapidly recruited and substantially contribute to the scar population adjacent to the repair site.[32,52] Here, we found that TPC application reduced laminin immunostaining at all timepoints in both enthesis and tendon-scar regions. Interestingly, while early α-SMA immunostaining was decreased at d7 in the enthesis region, we detected no differences at subsequent timepoints or in the tendon-scar region. Similarly, overall cellular density was generally not affected, indicating that reduced laminin was not due to reduced numbers of scar-forming cells. As α-SMA-lineage cells originate from surrounding tissues (such as the bursa or bone marrow) rather than from the tendon itself [32,21], we propose that secreted factors from delivered TPCs may inhibit laminin synthesis by local cells. Identifying these factors will be the focus of future research.

As a major chondrogenic transcription factor, Sox9+ cells play a crucial role in forming the fibrocartilaginous layer of the supraspinatus enthesis.[18] After injury, enthesis fibrocartilage decreases, which impairs functional restoration.[15,40] Our analyses reveal an increased percentage of Sox9+ fibrocartilage cells at the neo-enthesis site with TPC treatment, but only at d7. The increase was not sustained and qualitative fibrocartilage analysis by Toluidine Blue staining at d28 also did not show any difference with TPC treatment. Our findings regarding Sox9 are comparable to previously published results after rotator cuff repair augmented with bone marrow derived mesenchymal stem cells (BMSCs) in a rat model.[14] However, when BMSCs were transduced with the tendon transcription factor Scleraxis (which co-regulates Sox9 transcription), increased fibrocartilage formation was observed at 4 weeks postoperatively.[11,15] This suggests that the future of cell-augmentation lies in establishing a better understanding of the complex transcriptional and molecular cues underlying differentiation of progenitor cells. Unexpectedly, we detected a high percentage of Sox9+ cells in the distal tendon-scar regions (~40% of cells) in all groups, which might be an indicator of tendon degeneration and abnormal differentiation after injury.[32,33]

Forelimb gait analysis was previously found to be a highly reproducible functional assessment after murine rotator cuff repairs.[2,46,47] Here, TPC-treated mice demonstrated full recovery of gait properties while the fibrin-only control group remained functionally impaired. Furthermore, TPC application led to greater stride length and longer stance times than the fibrin-only group suggesting improved shoulder function and ability to bear weight. Although we expected improved enthesis biomechanics based on gait recovery, direct tensile testing showed no differences between fibrin-only and TPC-treatment for all biomechanical parameters and all parameters remained significantly impaired compared to intact controls. The discrepancy between gait and tissue biomechanics suggests there may be compensation of the anatomical shoulder unit that may improve overall gait with TPC treatment, despite persistent defects in tissue properties. This may further suggest that gait as a functional assay likely does not reflect direct enthesis strength, but encompasses additional factors associated with the surgery and healing. Improved gait due to TPC delivery may therefore also reflect improved healing of these other structures. Alternatively, it is possible that restoration of a normal enthesis is not required for normal gait recovery.

Although we expected that TPCs would directly contribute to the healing tissue via differentiation and integration, few labeled cells were detected at d7 and the majority was found near the deltoid and bursa. This suggests that the beneficial effects of TPC delivery may be due to paracrine signaling rather than direct differentiation. Despite minimal presence of labeled TPCs at d7, improvements in functional gait, scar formation, and collagen orientation were sustained at later stages, indicating that early alterations in the injury environment were sufficient to drive the course of healing. One potential mechanism may be the regulation of the immune response to injury. While numerous studies showed that BMSCs exert anti-inflammatory effects,[36,50] there are almost no studies that directly test the anti-inflammatory capacity of TPCs. One intriguing study showed that connective tissue growth factor treatment enhanced the anti-inflammatory function of perivascular-derived adult TPCs, which improved tendon healing after injury.[41] Although we found no difference in macrophage number, we did not investigate macrophage polarization; therefore, it could be that there are differences in pro-inflammatory and anti-inflammatory macrophages with TPC-treatment. Future studies will test the direct and indirect roles of TPCs in regulating the immune environment after rotator cuff repair.

While we consider it likely that TPC activity is mostly paracrine, we cannot fully rule out that some TPCs did in fact engraft and differentiate since overall Ad-Cre labeling efficiency was in the ~30% range and many cells were not labeled. This technical limitation may be overcome by enriching RosaT+ cells using fluorescence-activated cell sorting prior to delivery. Alternative labeling methods can also be used, such as *in vivo* genetic labeling prior to TPC isolation. On the other hand, limited engraftment may also be due to the initial placement of the bead at the greater tuberosity during the surgical procedure which may limit direct engraftment into the enthesis. Future research directions may include developing injectable cell delivery systems that better target the enthesis site.

Limitations in this study includes the surgical procedure. Acute tendon detachment of a healthy tendon does not reflect the chronic tendon degeneration observed in the human population; in mice, this surgical procedure also does not result in muscle atrophy and

fatty infiltration, which are additional clinical outcomes. Although this surgical model was consistent across the two treatment groups, thus allowing intergroup comparisons, future work will determine the effect of cell delivery on muscle outcomes, using a delayed (≥ 6 weeks) repair model.[46] For the repair itself, a singular bone tunnel was used whereas others have described the use of two divergent tunnels to better approximate the tendon reattachment to the native mouse supraspinatus insertion and potentially reduce the risk of eccentric loading.[27] While we concur with this rationale, we found relatively minimal lateralization of the neo-enthesis (200 μm) in comparison to the native enthesis and this was a consistent finding. Furthermore, no repair failures or tendon retractions were observed both in gross inspection and histological analyses. Since outcomes of a control group without fibrin-gel application were not assessed, we cannot reliably postulate regarding a potential effect of the delivery vehicle itself. Also, while neonatal TPC-treatment showed several critical improvements in healing compared to fibrin-only, direct comparison to adult TPC-treatment would be required to test whether these effects are specific to neonatal cells. The use of semi-quantitative immunofluorescence is also a limitation, compared to more quantitative measures such as Western blot, ELISA, or real time quantitative polymerase chain reaction. This was due to the very small amount of tissue that could be harvested from the mouse enthesis. Technologies such as laser capture microscopy could be used to overcome this limitation. Finally, the direct clinical applicability of neonatal cells for regenerative medicine is likely limited by ethical considerations as well as potential source of cells. However, feasible sources such as human induced pluripotent stem cells or BMSCs can be engineered or differentiated to recapitulate neonatal phenotypes, once the biology is better elucidated.

CONCLUSION

TPC delivery restored functional gait relative to fibrin-only gels after supraspinatus repair. Functional improvement with TPCs may be due to reduction in overall scar formation, improved early enthesis fibrocartilage formation, enhanced enthesis collagen orientation and altered bony composition response after tendon repair. Despite these improvements, there was no structural regeneration of the new enthesis and engraftment of the applied cells at the repair site was not observed. The beneficial effects of TPC delivery may be due to paracrine signaling rather than direct contribution to repair. Future work will determine the factors secreted by TPCs to develop translational targets and elucidate the mechanisms by which TPCs enhance healing.

Supplementary Material

Refer to Web version on PubMed Central for supplementary material.

Acknowledgments:

The authors acknowledge Bhavita Walia, Samantha Schnall, Deepak Kaji, Angela Montero, and Varun Arvind for their technical assistance and advice for these studies.

Funding:

These studies were supported by funding from the National Institutes of Health (R01AR069537, to A.H.H.), the European Society for Surgery of the Shoulder and Elbow (SECEC-ESSSE) Basic Science Research Grant to A.V., and the Belgian Orthopaedic and Traumatology Association (BVOT) Research Grant to A.V.

REFERENCES

1. Ahmad S, Haber M, Bokor DJ. The influence of intraoperative factors and postoperative rehabilitation compliance on the integrity of the rotator cuff after arthroscopic repair. J. Shoulder Elbow Surg. 2015;24(2):229–235. Available from: 10.1016/j.jse.2014.06.050 [PubMed: 25240808]
2. Bell R, Taub P, Cagle P, Flatow EL, Andarawis-Puri N. Development of a mouse model of supraspinatus tendon insertion site healing. J. Orthop. Res. 2015;33(1):25–32. doi:10.1002/jor.22727 [PubMed: 25231092]
3. Boudaoud A, Burian A, Borowska-Wykręt D, Uyttewaal M, Wrzalik R, Kwiatkowska D, et al. FibrilTool, an ImageJ plug-in to quantify fibrillar structures in raw microscopy images. Nat. Protoc. 2014;9(2):457–463. doi:10.1038/nprot.2014.024 [PubMed: 24481272]
4. Brochin RL, Zastrow R, Hussey-Andersen L, Parsons BO, Cagle PJ. Revision rotator cuff repair: a systematic review. J. Shoulder Elbow Surg. 2020;29(3):624–633. Available from: 10.1016/j.jse.2019.06.023 [PubMed: 31473134]
5. Buie HR, Campbell GM, Klinck RJ, MacNeil JA, Boyd SK. Automatic segmentation of cortical and trabecular compartments based on a dual threshold technique for in vivo micro-CT bone analysis. Bone. 2007;41(4):505–515. doi:10.1016/j.bone.2007.07.007 [PubMed: 17693147]
6. Carballo CB, Lebaschi A, Rodeo SA. Cell-based Approaches for Augmentation of Tendon Repair. Tech. Shoulder Elbow Surg. 2017;18(3):e6–e14. doi:10.1097/BTE.0000000000000132
7. Chahal J, Van Thiel GS, Mall N, Heard W, Bach BR, Cole BJ, et al. . The role of platelet-rich plasma in arthroscopic rotator cuff repair: A systematic review with quantitative synthesis. Arthrosc. - J. Arthrosc. Relat. Surg. 2012;28(11):1718–1727. Available from: 10.1016/j.arthro.2012.03.007
8. Choi S, Kim MK, Kim GM, Roh YH, Hwang IK, Kang H. Factors associated with clinical and structural outcomes after arthroscopic rotator cuff repair with a suture bridge technique in medium, large, and massive tears. J. Shoulder Elbow Surg. 2014;23(11):1675–1681. Available from: 10.1016/j.jse.2014.02.021 [PubMed: 24862247]
9. Chung SW, Oh JH, Gong HS, Kim JY, Kim SH. Factors affecting rotator cuff healing after arthroscopic repair: Osteoporosis as one of the independent risk factors. Am. J. Sports Med. 2011;39(10):2099–2107. doi:10.1177/0363546511415659 [PubMed: 21813440]
10. Derwin KA, Galatz LM, Ratcliffe A, Thomopoulos S. Orthopaedic. 2018;109:1–7.
11. Furumatsu T, Shukunami C, Amemiya-Kudo M, Shimano H, Ozaki T. Scleraxis and E47 cooperatively regulate the Sox9-dependent transcription. Int. J. Biochem. Cell Biol. 2010;42(1):148–156. doi:10.1016/j.biocel.2009.10.003 [PubMed: 19828133]
12. Galatz LM, Ball CM, Teefey SA, Middleton WD, Yamaguchi K. The Outcome and Repair Integrity of Completely Arthroscopically Repaired Large and Massive Rotator Cuff Tears. J. Bone Jt. Surg. - Ser. A. 2004;86(2):219–224. doi:10.2106/00004623-200402000-00002
13. Galatz LM, Charlton N, Das R, Kim HM, Havlioglu N, Thomopoulos S. Complete removal of load is detrimental to rotator cuff healing. J. Shoulder Elbow Surg. 2009;18(5):669–675. Available from: 10.1016/j.jse.2009.02.016 [PubMed: 19427237]
14. Gulotta LV, Kovacevic D, Ehteshami JR, Dagher E, Packer JD, Rodeo SA. Application of bone marrow-derived mesenchymal stem cells in a Rotator cuff repair model. Am. J. Sports Med. 2009;37(11):2126–2133. doi:10.1177/0363546509339582 [PubMed: 19684297]
15. Gulotta LV, Kovacevic D, Packer JD, Deng XH, Rodeo SA Bone marrow-derived mesenchymal stem cells transduced with scleraxis improve rotator cuff healing in a rat model. Am. J. Sports Med. 2011;39(6):1282–1289. doi:10.1177/0363546510395485 [PubMed: 21335341]
16. Hernigou P, Flouzat Lachaniette CH, Delambre J, Zilber S, Duffiet P, Chevallier N, et al. . Biologic augmentation of rotator cuff repair with mesenchymal stem cells during arthroscopy improves healing and prevents further tears: A case-controlled study. Int. Orthop. 2014;38(9):1811–1818. doi:10.1007/s00264-014-2391-1 [PubMed: 24913770]

17. Howell K, Chien C, Bell R, Laudier D, Tufa SF, Keene DR, et al. Novel Model of Tendon Regeneration Reveals Distinct Cell Mechanisms Underlying Regenerative and Fibrotic Tendon Healing. Sci. Rep. 2017;7(March):1–14. Available from: 10.1038/srep45238 [PubMed: 28127051]
18. Jensen PT, Lambertsen KL, Frich LH. Assembly, maturation, and degradation of the supraspinatus enthesis. J. Shoulder Elbow Surg. 2018;27(4):739–750. Available from: 10.1016/j.jse.2017.10.030 [PubMed: 29329904]
19. Jost B, Zumstein M, Pfirrmann CWA, Gerber C. Long-term outcome after structural failure of rotator cuff repairs. J. Bone Jt. Surg. - Ser. A. 2006;88(3):472–479. doi:10.2106/JBJS.E.00003
20. Junqueira LC, Bignolas G, Brentani RR. Picrosirius staining plus polarization microscopy, a specific method for collagen detection in tissue sections. Histochem. J. 1979 Jul;11(4):447–55. Available from: 10.1007/BF01002772 [PubMed: 91593]
21. Kida Y, Morihara T, Matsuda KI, Kajikawa Y, Tachiiri H, Iwata Y, et al. Bone marrow-derived cells from the footprint infiltrate into the repaired rotator cuff. J. Shoulder Elbow Surg. 2013;22(2):197–205. Available from: 10.1016/j.jse.2012.02.007 [PubMed: 22543003]
22. Killian ML, Cavinatto L, Galatz LM, Thomopoulos S. The role of mechanobiology in tendon healing. J. Shoulder Elbow Surg. 2012;21(2):228–237. Available from: 10.1016/j.jse.2011.11.002 [PubMed: 22244066]
23. Kowalsky MS, Keener JD. Revision arthroscopic rotator cuff repair: Repair integrity and clinical outcome - Surgical technique. J. Bone Jt. Surg. - Ser. A. 2011;93(SUPPL. 1):62–74. doi:10.2106/JBJS.J.01173
24. Kurtaliaj I, Golman M, Abraham AC, Thomopoulos S. Biomechanical testing of murine tendons. J. Vis. Exp. 2019;2019(152):1–12. doi:10.3791/60280
25. Kwon J, Kim SH, Lee YH, Kim TI, Oh JH. The Rotator Cuff Healing Index: A New Scoring System to Predict Rotator Cuff Healing After Surgical Repair. Am. J. Sports Med. 2019;47(1):173–180. doi:10.1177/0363546518810763 [PubMed: 30485753]
26. Le BTN, Wu XL, Lam PH, Murrell GAC. Factors predicting rotator cuff retears: An analysis of 1000 consecutive rotator cuff repairs. Am. J. Sports Med. 2014;42(5):1134–1142. doi:10.1177/0363546514525336 [PubMed: 24748610]
27. Lebaschi AH, Deng XH, Camp CL, Zong J, Cong GT, Carballo CB, et al. Biomechanical, Histologic, and Molecular Evaluation of Tendon Healing in a New Murine Model of Rotator Cuff Repair. Arthrosc. - J. Arthrosc. Relat. Surg. 2018;34(4):1173–1183. doi:10.1016/j.arthro.2017.10.045
28. Lorbach O, Bachelier F, Vees J, Kohn D, Pape D. Cyclic loading of rotator cuff reconstructions: Single-row repair with modified suture configurations versus double-row repair. Am. J. Sports Med. 2008;36(8):1504–1510. doi:10.1177/0363546508314424 [PubMed: 18296541]
29. Lu HH, Thomopoulos S. Functional attachment of soft tissues to bone: Development, healing, and tissue engineering. Annu. Rev. Biomed. Eng. 2013;15:201–226. doi:10.1146/annurev-bioeng-071910-124656 [PubMed: 23642244]
30. Madisen L, Zwingman TA, Sunkin SM, Oh SW, Zariwala HA, Gu H, et al. A robust and high-throughput Cre reporting and characterization system for the whole mouse brain. Nat. Neurosci. 2010;13(1):133–140. Available from: 10.1038/nn.2467 [PubMed: 20023653]
31. McElvany MD, McGoldrick E, Gee AO, Neradilek MB, Matsen FA. Rotator cuff repair: Published evidence on factors associated with repair integrity and clinical outcome. Am. J. Sports Med. 2015;43(2):491–500. doi:10.1177/0363546514529644 [PubMed: 24753240]
32. Moser HL, Abraham AC, Howell K, Laudier D, Zumstein MA, Galatz LM, et al. Cell lineage tracing and functional assessment of supraspinatus tendon healing in an acute repair murine model. J. Orthop. Res. 2021;39(8):1789–1799. Available from: 10.1002/jor.24769 [PubMed: 32497311]
33. Moser HL, Doe AP, Meier K, Garnier S, Laudier D, Akiyama H, et al. Genetic lineage tracing of targeted cell populations during enthesis healing. J. Orthop. Res. 2018;36(12):3275–3284. doi:10.1002/jor.24122 [PubMed: 30084210]
34. Nakamura H, Gotoh M, Mitsui Y, Honda H, Ohzono H, Shimokobe H, et al. Factors Affecting Clinical Outcome in Patients with Structural Failure after Arthroscopic Rotator Cuff Repair. Arthrosc. - J. Arthrosc. Relat. Surg. 2016;32(5):732–739. Available from: 10.1016/j.arthro.2015.11.025

35. Patel S, Gualtieri AP, Lu HH, Levine WN. Advances in biologic augmentation for rotator cuff repair. Ann. N. Y. Acad. Sci. 2016;1383(1):97–114. doi:10.1111/nyas.13267 [PubMed: 27750374]
36. Pittenger MF, Discher DE, Péault BM, Phinney DG, Hare JM, Caplan AI. Mesenchymal stem cell perspective: cell biology to clinical progress. npj Regen. Med. 2019;4(1). Available from: 10.1038/s41536-019-0083-6
37. Pogorzelski J, Godin JA, Fritz EM, Cinque ME, Chahla J, Huard J, et al. The use of biological approaches in the treatment of shoulder pathology a critical analysis review. JBJS Rev. 2017;5(9):1–7. doi:10.2106/JBJS.RVW.17.00035
38. Rodeo SA. Biologic augmentation of rotator cuff tendon repair. J. Shoulder Elbow Surg. 2007;16(5 SUPPL.):191–197. doi:10.1016/j.jse.2007.03.012
39. Schwartz AG, Galatz LM, Thomopoulos S. Enthesis regeneration: A role for Gli1+ progenitor cells. Dev. 2017;144(7):1159–1164. doi:10.1242/dev.139303
40. Shah SA, Kormpakis I, Havlioglu N, Ominsky MS, Galatz LM, Thomopoulos S. Sclerostin antibody treatment enhances rotator cuff tendon-to-bone healing in an animal model. J. Bone Jt. Surg. - Am. Vol. 2017;99(10):855–864. doi:10.2106/JBJS.16.01019
41. Tarafder S, Chen E, Jun Y, Kao K, Sim KH, Back J, et al. Tendon stem/progenitor cells regulate inflammation in tendon healing via JNK and STAT3 signaling. FASEB J. 2017;31(9):3991–3998. doi:10.1096/fj.201700071R [PubMed: 28533328]
42. Tokunaga T, Shukunami C, Okamoto N, Taniwaki T, Oka K, Sakamoto H, et al. FGF-2 Stimulates the Growth of Tenogenic Progenitor Cells to Facilitate the Generation of Tenomodulin -Positive Tenocytes in a Rat Rotator Cuff Healing Model. Am. J. Sports Med. 2015;43(10):2411–2422. doi:10.1177/0363546515597488 [PubMed: 26311443]
43. Varghese F, Bukhari AB, Malhotra R, De A. IHC profiler: An open source plugin for the quantitative evaluation and automated scoring of immunohistochemistry images of human tissue samples. PLoS One. 2014;9(5). doi:10.1371/journal.pone.0096801
44. Walia B, Huang AH. Tendon stem progenitor cells: Understanding the biology to inform therapeutic strategies for tendon repair. J. Orthop. Res. 2019;37(6):1270–1280. doi:10.1002/jor.24156 [PubMed: 30270569]
45. Wall LB, Keener JD, Brophy RH. Double-row vs single-row rotator cuff repair: A review of the biomechanical evidence. J. Shoulder Elbow Surg. 2009;18(6):933–941. Available from: 10.1016/j.jse.2009.07.002 [PubMed: 19833290]
46. Wang Z, Liu X, Davies MR, Horne D, Kim H, Feeley BT. A Mouse Model of Delayed Rotator Cuff Repair Results in Persistent Muscle Atrophy and Fatty Infiltration. Am. J. Sports Med. 2018;46(12):2981–2989. doi:10.1177/0363546518793403 [PubMed: 30198747]
47. Wang Z, Liu X, Jiang K, Kim H, Kajimura S, Feeley BT Intramuscular Brown Fat Activation Decreases Muscle Atrophy and Fatty Infiltration and Improves Gait After Delayed Rotator Cuff Repair in Mice. Am. J. Sports Med. 2020;48(7):1590–1600. doi:10.1177/0363546520910421 [PubMed: 32282238]
48. Willinger L, Lacheta L, Beitzel K, Buchmann S, Woertler K, Imhoff AB, et al. Clinical Outcomes, Tendon Integrity, and Shoulder Strength After Revision Rotator Cuff Reconstruction: A Minimum 2 Years' Follow-up. Am. J. Sports Med. 2018;46(11):2700–2706. doi:10.1177/0363546518786006 [PubMed: 30084649]
49. Wu XL, Briggs L, Murrell GAC. Intraoperative determinants of rotator cuff repair integrity: An analysis of 500 consecutive repairs. Am. J. Sports Med. 2012;40(12):2771–2776. doi:10.1177/0363546512462677 [PubMed: 23104609]
50. Yagi H, Soto-Gutierrez A, Parekkadan B, Kitagawa Y, Tompkins RG, Kobayashi N, et al. Mesenchymal stem cells: Mechanisms of immunomodulation and homing. Cell Transplant. 2010;19(6–7):667–679. doi:10.3727/096368910X508762 [PubMed: 20525442]
51. Yang J, Robbins M, Reilly J, Maerz T, Anderson K. The Clinical Effect of a Rotator Cuff Retear. Am. J. Sports Med. 2017;45(3):733–741. doi:10.1177/0363546516652900 [PubMed: 27416991]
52. Yoshida R, Alaee F, Dyrna F, Kronenberg MS, Maye P, Kalajzic I, Rowe DW, Mazzocca AD DN. Murine supraspinatus tendon injury model to identify the cellular origins of rotator cuff healing. Connect Tissue Res 2016;57:507–515. doi: 10.1080/03008207.2016.1189910. [PubMed: 27184388]

53. Zumstein MA, Jost B, Hempel J, Hodler J, Gerber C. The clinical and structural long-term results of open repair of massive tears of the rotator cuff. J. Bone Jt. Surg. - Ser. A. 2008;90(11):2423–2431. doi:10.2106/JBJS.G.00677

54. Zumstein MA, Lädermann A, Raniga S, Schär MO. The biology of rotator cuff healing. Orthop. Traumatol. Surg. Res. 2017;103(1):S1–S10. Available from: 10.1016/j.otsr.2016.11.003 [PubMed: 28043853]

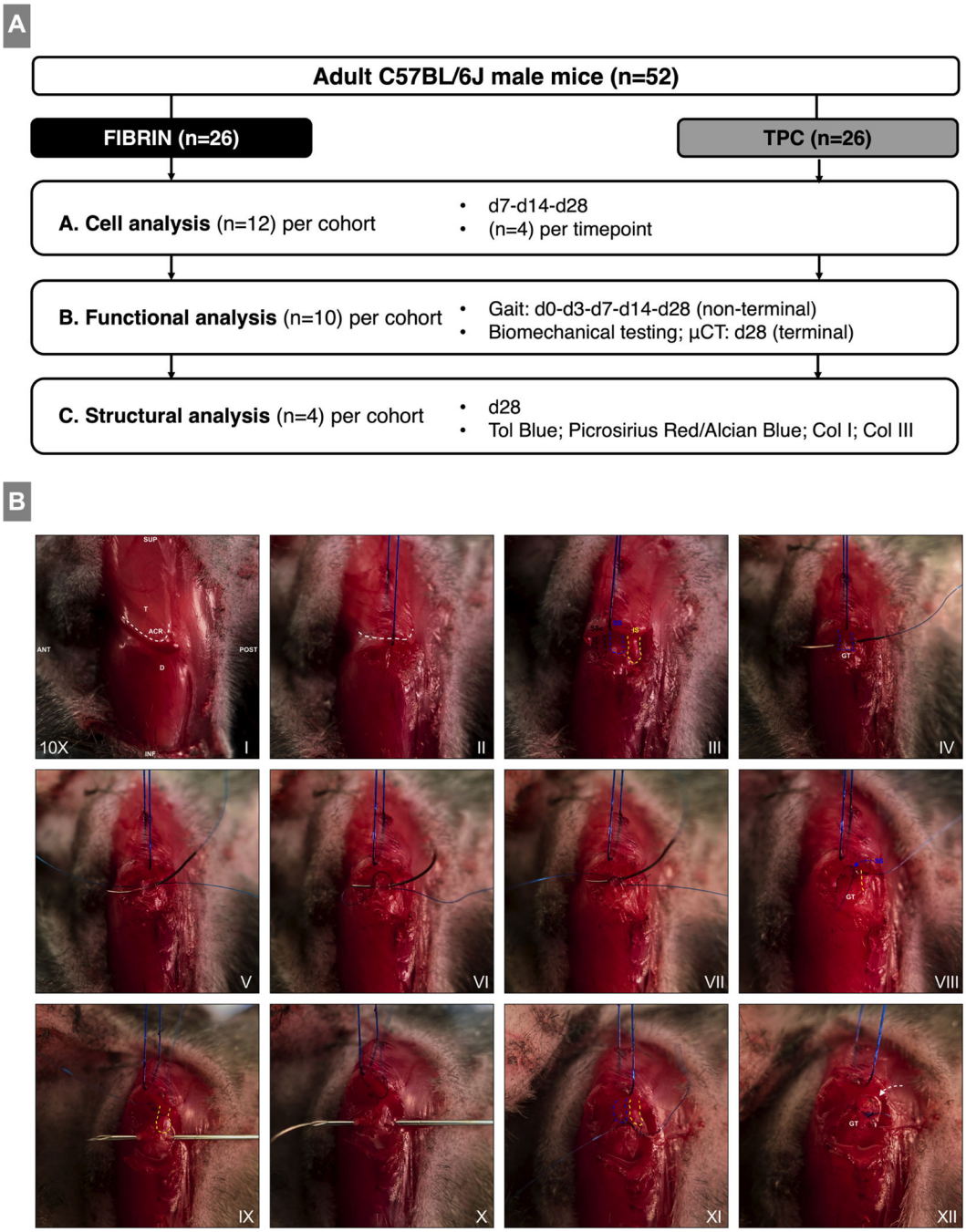

Figure 1: Study design and intraoperative imaging of the surgical procedure.

(A) Experimental study design and treatment groups. (B) Surgical procedure for supraspinatus tendon detachment, fibrin gel delivery, and repair. (I) Anatomic overview after skin incision. (II) Horizontal incision of deltoid. (III) Additional exposure was obtained for imaging purposes to visualize the subscapularis, supraspinatus and infraspinatus tendons. (IV-VII) The supraspinatus tendon is secured with a modified figure 8 stitch to obtain equal pulling tension on the tendon. (VIII) Sharp detachment of the tendon from the greater tuberosity. (IX) Posterior to anterior bone tunnel. (X) Suture is passed via the 30G needle

from anterior to posterior. (XI) Suture is tied and tensioned to closely approximate the native insertion site. (XII) Fibrin gel bead (white arrow) is added to the enthesis region. BioM: Biomechanical testing; μCT: Micro-CT imaging; T: Trapezius muscle; ACR: Acromion; D: Deltoid muscle; SSc: Subscapularis tendon; SS: Supraspinatus tendon; IS: Infraspinatus tendon; GT: Greater tuberosity. Images were taken at 10x magnification.

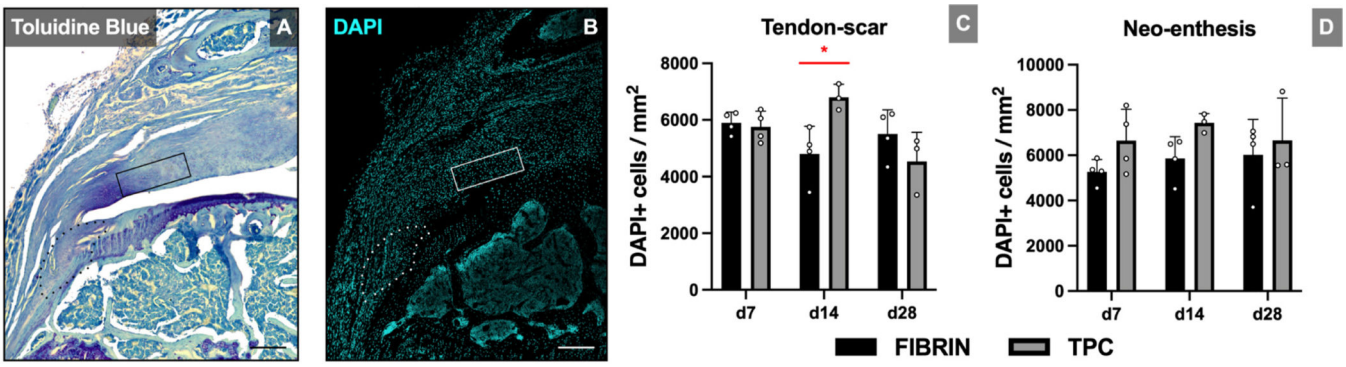

Figure 2: DAPI staining shows transient or no changes in cellularity with TPC delivery.

(A) Toluidine blue staining identifies ROIs for the neo-enthesis (dotted outline) and tendon-scar (solid rectangle). (B) DAPI staining of adjacent sections and (C, D) quantification for cellularity. Significant increase in cellularity was only detected at d14 in the tendon-scar ROI. Scale bars = 100 μm. * p≤0.05.

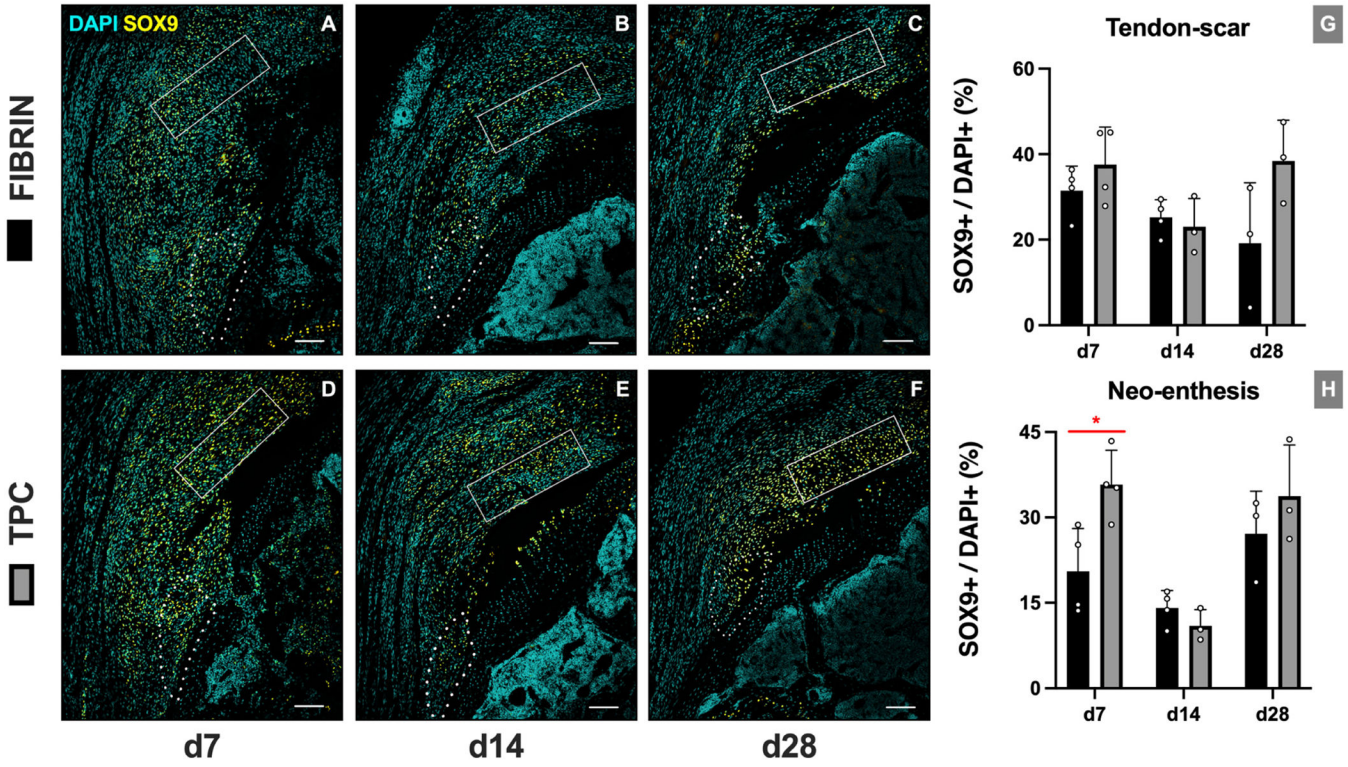

Figure 3: TPC delivery transiently increases neo-enthesis SOX9+ fibrocartilage cells.

Representative images of Sox9 immunostaining for (A-C) fibrin-only and (D-F) TPC-treated mice. (G, H) Quantification shows increase in neo-enthesis Sox9+ cells at d7 but not d14 and d28 with TPC delivery. Dotted outline and solid rectangle indicate neo-enthesis and tendon-scar regions, respectively. Scale bars = 200 μm. * p≤0.05.

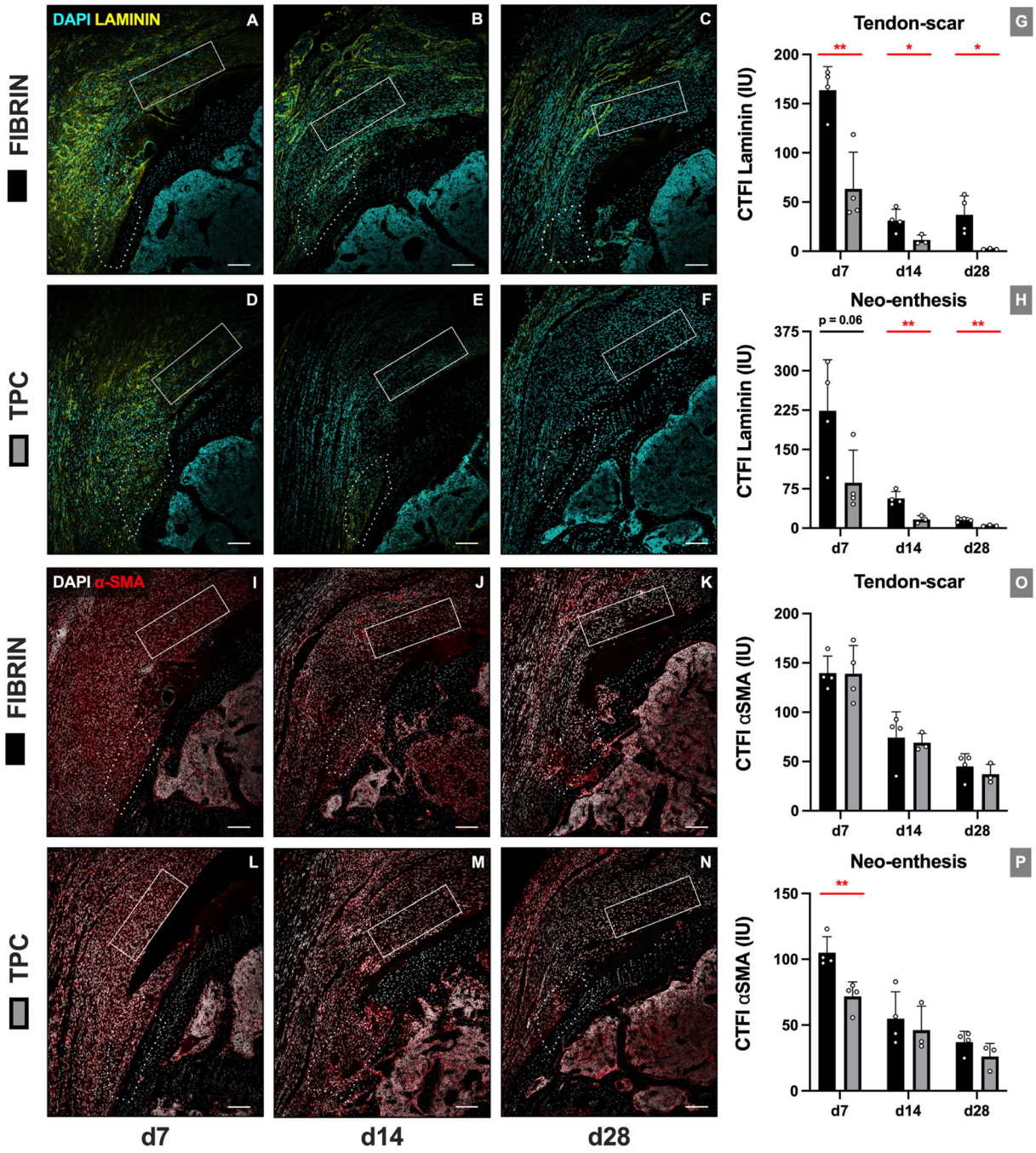

Figure 4: TPC delivery resulted in reduced scar formation and transiently reduced enthesis scar-forming cells.

(A-F) Representative images and (G, H) quantification for laminin immunostaining. (I-N) Representative images and (O, P) quantification for α-SMA immunostaining. Dotted outline and solid rectangle indicate neo-enthesis and tendon-scar regions, respectively. Scale bars = 200 μm. * p≤0.05; ** p≤0.01.

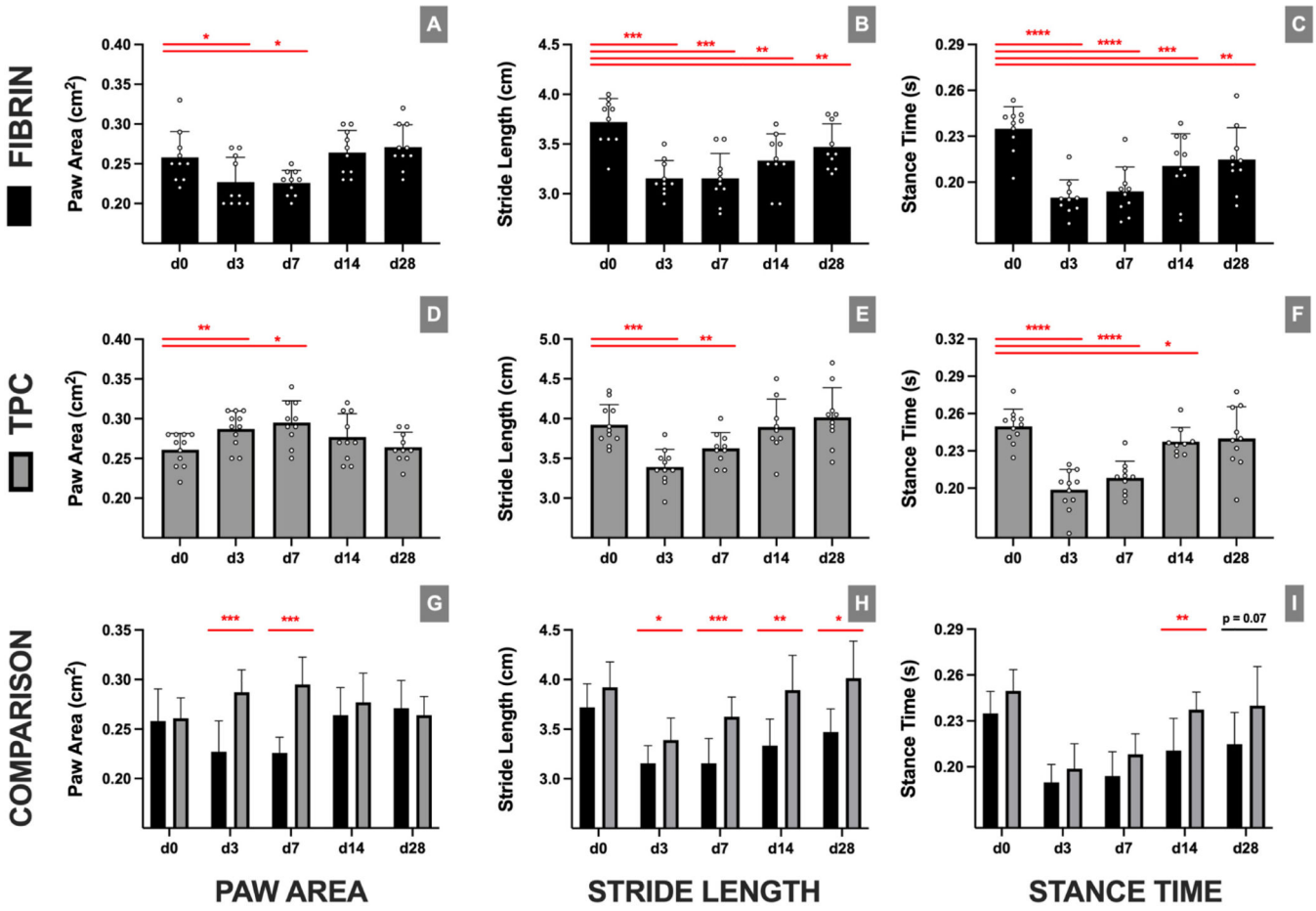

Figure 5: TPC delivery resulted in full recovery of functional gait.

Gait parameters for (A-C) fibrin-only and (D-F) TPC treatment over time. (G-I) Direct comparisons between fibrin-only and TPC treatment for each timepoint reveal significant differences for all gaitparameters at different timepoints. exhibited restoration of their gait parameters relative to preoperative measurements by 4 weeks postoperatively. * p≤0.05; ** p≤0.01; *** p≤0.001; **** p≤0.0001.

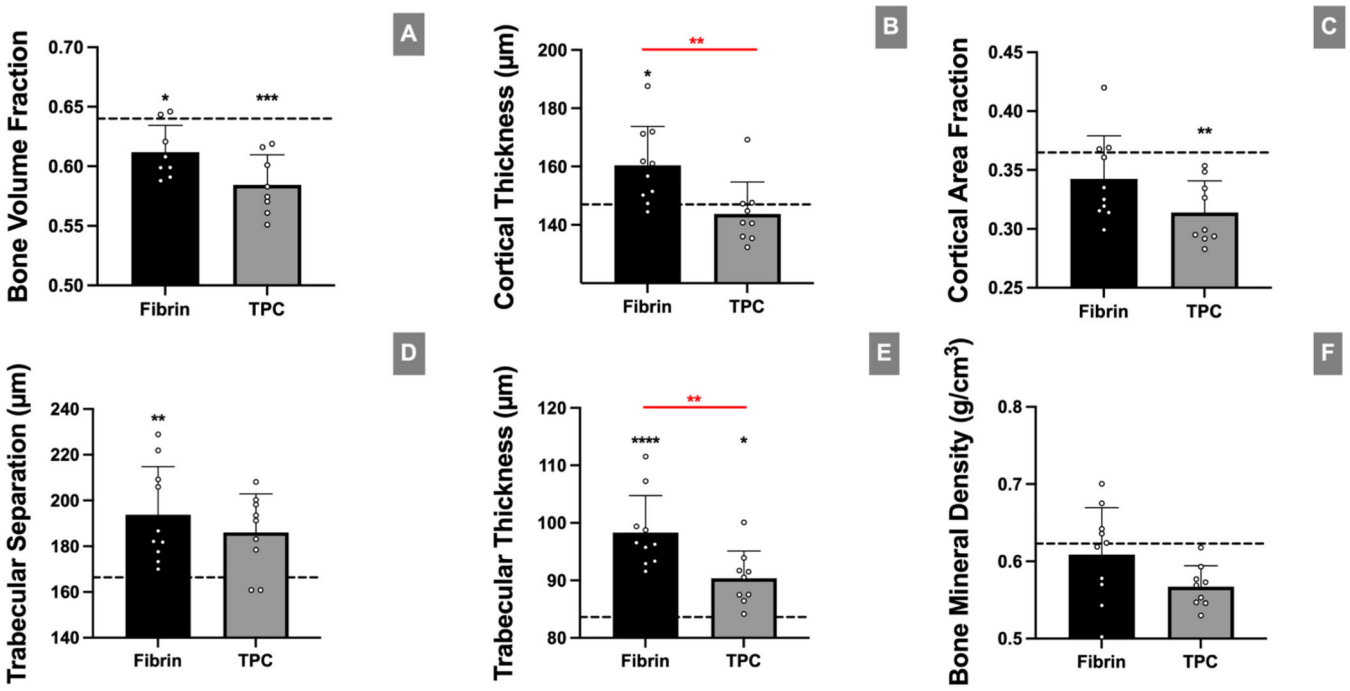

Figure 6: TPC delivery resulted in improved cortical and trabecular bone thickness compared with the fibrin-only control group.

(A-F) µCT analyses of bone parameters with fibrin-only and TPC treatment after injury. Higher postoperative differences were found at 4 weeks in fibrin than TPC treated mice for cortical and trabecular thickness, respectively. Dotted lines in graphs represent mean values of uninjured samples (n=10). asterisks indicate significant difference between mean value of uninjured samples and respective treatment group. * $p \leq 0.05$; ** $p \leq 0.01$; *** $p \leq 0.001$; **** $p \leq 0.0001$.

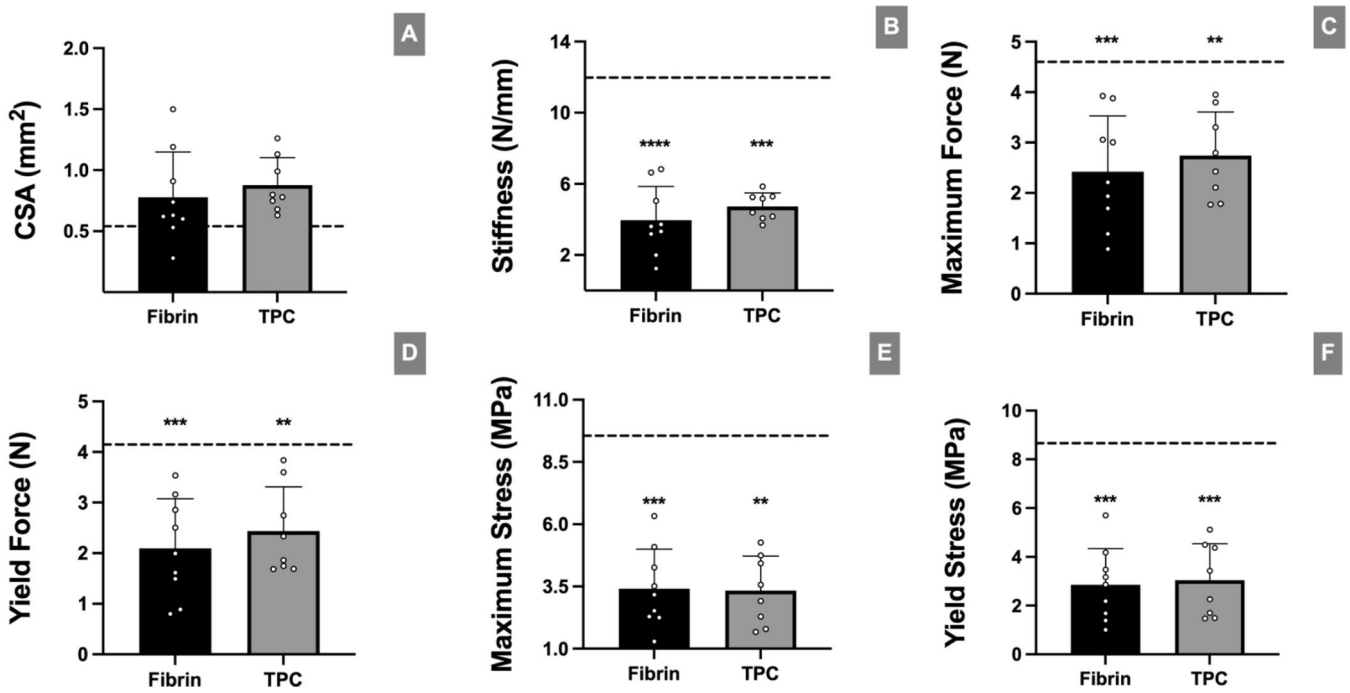

Figure 7: TPC delivery failed to effectively restore tendon tensile and material properties after repair.

(A) Cross-sectional area measurement of enthesis footprint obtained from μCT. (B-F) Biomechanical analyses of attachment properties with fibrin-only and TPC treatment after injury. No significant differences were found between the surgical groups. Dotted lines in graphs represent mean values of uninjured samples (n=10). Black asterisks indicate significant difference between mean value of uninjured samples and respective treatment groups. * $p \leq 0.05$; ** $p \leq 0.01$; *** $p \leq 0.001$.

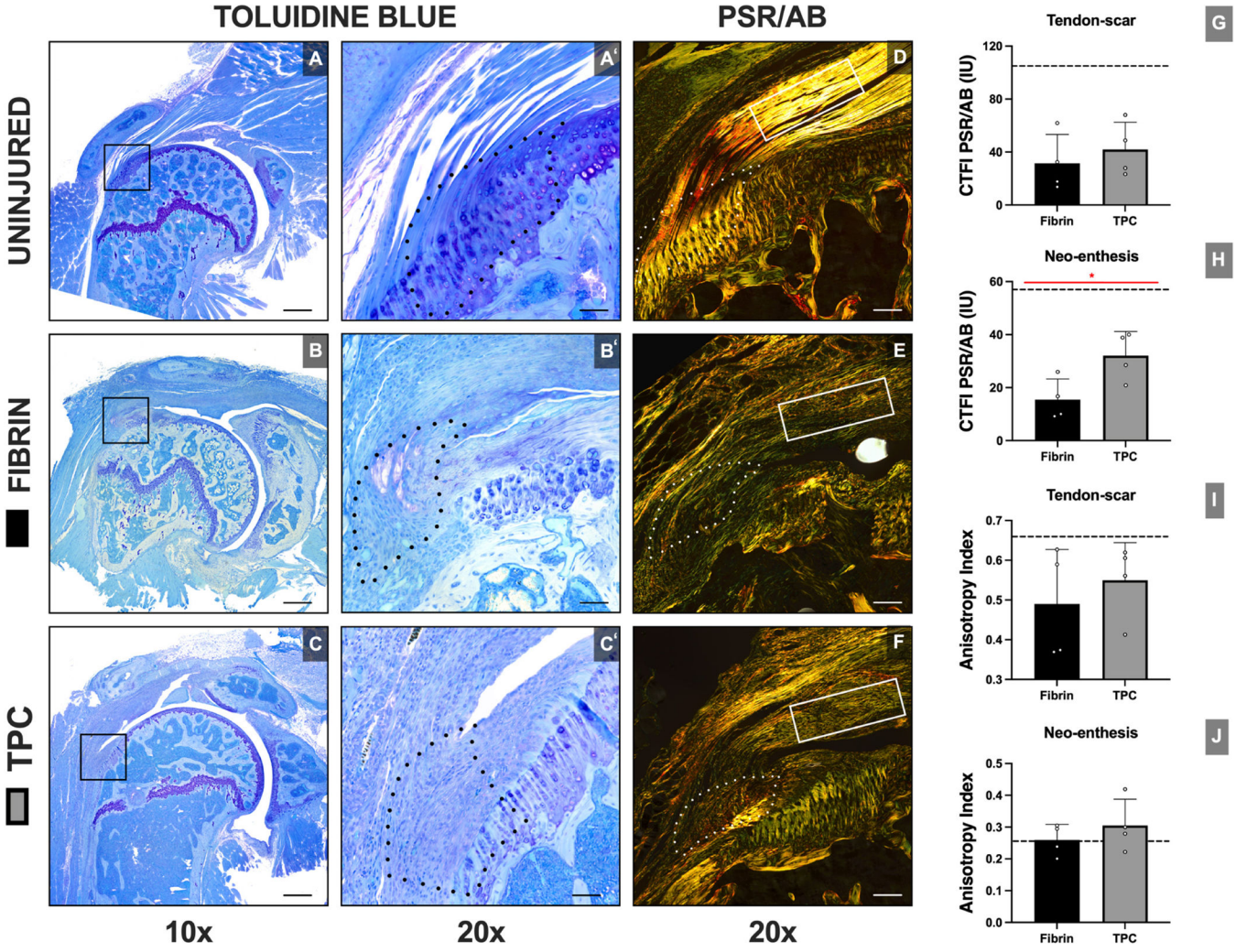

Figure 8: TPC delivery improves collagen orientation compared to fibrin-only treatment at the neo-enthesis site.

Structural analysis with Toluidine Blue (A-C) and Picrosirius Red/Alcian Blue (D-F) staining with quantifications of collagen orientation (G-J). Dotted outline and solid rectangle in images indicate neo-enthesis and tendon-scar regions, respectively. Dotted lines in graphs represent mean value of uninjured sample. CTFI: Corrected total fluorescence intensities. Black scale bars = 800 μm and 200 μm for 10x and 20x magnification, respectively. White scale bars = 400 μm. *, p≤0.05.

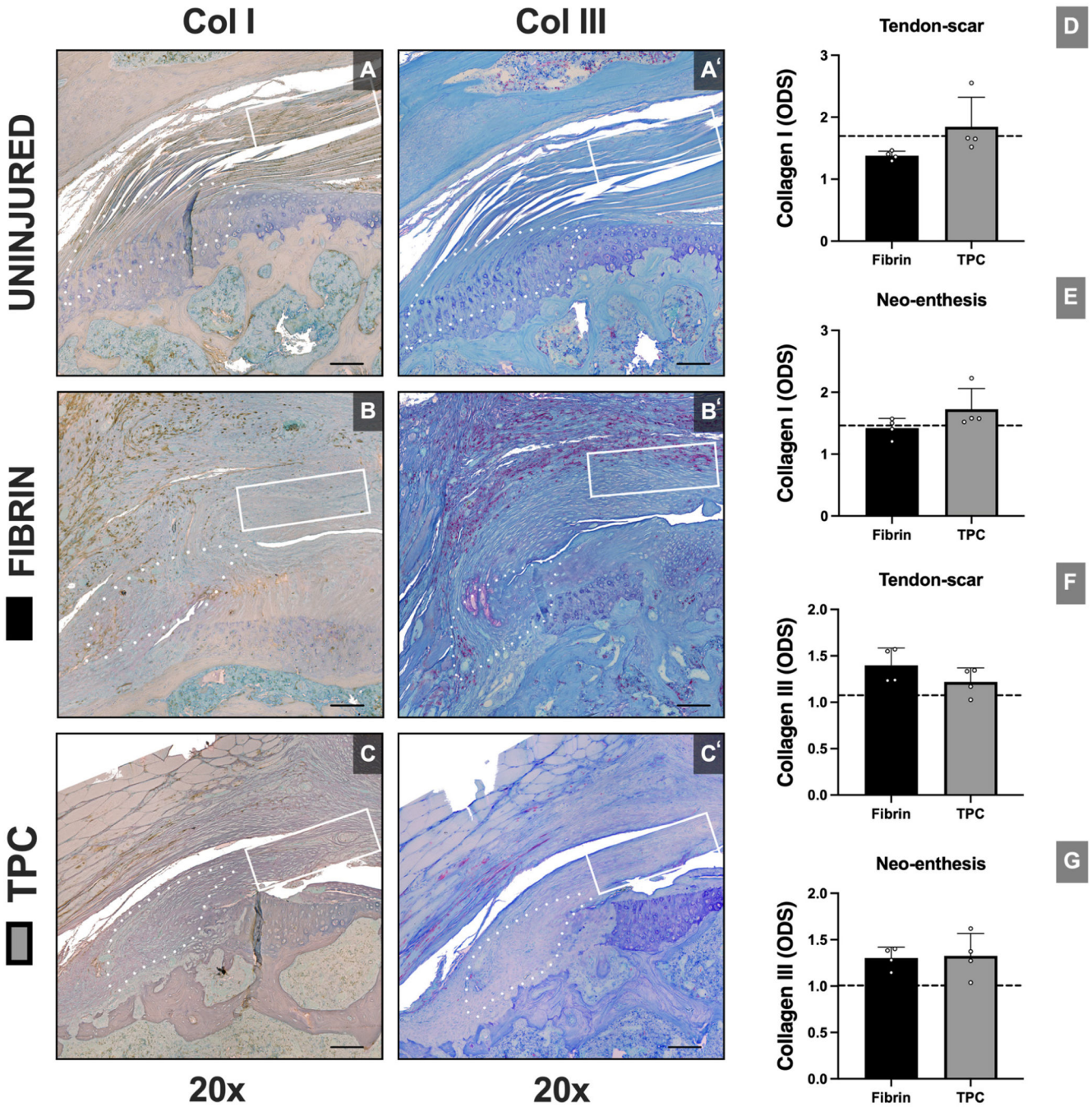

Figure 9: No differences observed in collagen type I and type III quantification with TPC delivery.

Structural analysis with collagen I (A-C) and collagen III (A'-C') staining with optical density score (ODS) quantifications (D-G). Dotted outline and solid rectangle in images indicate neo-enthesis and tendon-scar regions, respectively. Dotted lines in graphs represent mean value of uninjured sample. ODS: Optical density score. Scale bars = 400 μm.

Table 1:

Parameters used for power analysis calculations.

Assay	Difference in Means	Coefficient of Variation	Minimum Sample Size
Cell and histological quantification	20%	10%	N=3
Gait Parameters	30%	20%	N=10
Mechanical Properties	60%	35%	N=6
MicroCT	10%	8%	N=6